Atmos. Meas. Tech., 8, 1575–1591, 2015
www.atmos-meas-tech.net/8/1575/2015/
doi:10.5194/amt-8-1575-2015

Atmospheric Measurement Techniques
Open Access

Towards validation of ammonia (NH_3) measurements from the IASI satellite

M. Van Damme[1,2], L. Clarisse[1], E. Dammers[2], X. Liu[3], J. B. Nowak[4,5,*], C. Clerbaux[1,6], C. R. Flechard[7], C. Galy-Lacaux[8], W. Xu[3], J. A. Neuman[4,5], Y. S. Tang[9], M. A. Sutton[9], J. W. Erisman[2,10], and P. F. Coheur[1]

[1]Spectroscopie de l'atmosphère, Chimie Quantique et Photophysique, Université Libre de Bruxelles, Brussels, Belgium
[2]Cluster Earth and Climate, Department of Earth Sciences, Vrije Universiteit Amsterdam, Amsterdam, the Netherlands
[3]College of Resources and Environmental Sciences, China Agricultural University, Beijing 100193, China
[4]Cooperative Institute for Research in Environmental Sciences, University of Colorado Boulder, Boulder, Colorado, USA
[5]Chemical Sciences Division, Earth System Research Laboratory, NOAA, Boulder, Colorado, USA
[6]UPMC; Université Versailles St. Quentin; CNRS/INSU, LATMOS-IPSL, Paris, France
[7]INRA, Agrocampus Ouest, UMR 1069 SAS, Rennes, France
[8]Laboratoire d'Aérologie, UMR 5560, Université Paul-Sabatier (UPS) and CNRS, Toulouse, France
[9]Centre for Ecology and Hydrology, Edinburgh Research Station, Bush Estate, Penicuik, Midlothian EH26 0QB, UK
[10]Louis Bolk Institute, Driebergen, the Netherlands
[*]now at: Aerodyne Research, Inc., Billerica, MA, USA

Correspondence to: M. Van Damme (martin.van.damme@ulb.ac.be)

Received: 22 September 2014 – Published in Atmos. Meas. Tech. Discuss.: 4 December 2014
Revised: 16 February 2015 – Accepted: 1 March 2015 – Published: 26 March 2015

Abstract. Limited availability of ammonia (NH_3) observations is currently a barrier for effective monitoring of the nitrogen cycle. It prevents a full understanding of the atmospheric processes in which this trace gas is involved and therefore impedes determining its related budgets. Since the end of 2007, the Infrared Atmospheric Sounding Interferometer (IASI) satellite has been observing NH_3 from space at a high spatio-temporal resolution. This valuable data set, already used by models, still needs validation. We present here a first attempt to validate IASI-NH_3 measurements using existing independent ground-based and airborne data sets. The yearly distributions reveal similar patterns between ground-based and space-borne observations and highlight the scarcity of local NH_3 measurements as well as their spatial heterogeneity and lack of representativity. By comparison with monthly resolved data sets in Europe, China and Africa, we show that IASI-NH_3 observations are in fair agreement, but they are characterized by a smaller variation in concentrations. The use of hourly and airborne data sets to compare with IASI individual observations allows investigations of the impact of averaging as well as the representativity of independent observations for the satellite footprint. The importance of considering the latter and the added value of densely located airborne measurements at various altitudes to validate IASI-NH_3 columns are discussed. Perspectives and guidelines for future validation work on NH_3 satellite observations are presented.

1 Introduction

Ammonia (NH_3) is a key component of our ecosystems and the primary form of reactive nitrogen (Nr) in the environment (Erisman et al., 2007; Sutton et al., 2013a). It represents more than half of Nr atmospheric emissions (Galloway, 2003a). Mainly released by food production, the drastic increase of NH_3 emission in the atmosphere in the last century was due to the need to feed an ever-growing population combined with greatly increased rates of livestock production (Erisman et al., 2008; Galloway et al., 2008). This increase has numerous environmental impacts on ecosystems (Sutton et al., 2008; Erisman et al., 2013). As the major basic species in the

atmosphere, NH_3 reacts rapidly with acid gases and drives the acidity of precipitations and particulate matter (Behera et al., 2013). Its role in aerosol formation (Hertel et al., 2012) makes it an important component in air quality and climate issues (Pope et al., 2009; Erisman et al., 2011). In addition to being directly toxic to plants at high concentrations (Krupa, 2003), NH_3 and its derivatives are also quickly deposited in the ecosystems, increasing their eutrophication and reducing biodiversity (Erisman et al., 2007; EEA-European Environment Agency, 2014). All these impacts are magnified as the nitrogen atom included in NH_3 enters the "nitrogen cascade" (Galloway et al., 2003b).

Human activities have caused a large increase of NH_3: manure management and agricultural soils are responsible for more than 82 % of the 49.3 Tg of NH_3 emitted globally in 2008 (EDGAR-Emission Database for Global Atmospheric Research, 2011). The second largest contribution is from biomass burning, mainly linked to large scale fires (6 Tg in 2008, following EDGAR v4.2 inventory) but also to a lesser extent to agricultural waste burning (0.76 Tg in 2008). It is worth noting that global emission inventories have an uncertainty of at least 30 % (Sutton et al., 2013a). The amount of NH_3 emitted in the atmosphere is also strongly dependent on agricultural practices and climatic conditions (Sutton et al., 2013a, b) and this causes large variability in emissions on national/regional scales (Reis et al., 2009). At a local scale, other sources such as traffic and/or industry can be important (Gong et al., 2011). A further increase of NH_3 emissions is expected during this century due to agricultural intensification and the projected increases in surface temperature, which favors NH_3 volatilization (Fiore et al., 2012; Sutton et al., 2013a).

Despite the importance of NH_3 for the environment, the atmospheric processes in which it is involved and the related budgets are still poorly understood (Fowler et al., 2013). Progress in instrumentation, flux measurements and understanding of processes during the last decades have allowed advances in local/regional modeling (Flechard et al., 2013). For example, the development of a bi-directional parameterization of surface/atmosphere exchange of NH_3 has improved regional modeling, for which the information needed as input (e.g., emission inventories, meteorological data) are well known (Wichink Kruit et al., 2012; Bash et al., 2013). More limitations exist on NH_3 modeling at global scale. As an example, in the multi-model comparison of Dentener et al. (2006), only 7 of 23 models included NH_x (Fowler et al., 2013). Even as the NH_3 cycle is more and more integrated in the simulations (e.g., see Hauglustaine et al., 2014), one of the key limitations for global modeling is still the availability of measurements across the globe.

Measuring NH_3 is indeed challenging because of (i) strong temporal and spatial variability of ambient levels, (ii) quick conversion of NH_3 from one phase to another (gas/particulate/liquid) and (iii) its stickiness to the observational instruments (Sutton et al., 2008; von Bobrutzki et al., 2010). There are currently very few monitoring stations that provide daily or hourly resolved NH_3 measurements, with most long-term monitoring of NH_3 being made using a passive sampler or dedicated denuder with a time resolution of several weeks. Some countries have their own network providing long-term ground-based observations (e.g., United States, Netherlands, United Kingdom) but these are the exception and most of the data sets are restricted to a certain period (e.g., NitroEurope data set (Flechard et al., 2011)). Therefore, the spatial coverage of these networks and campaigns is strongly heterogeneous, with the large majority of available measurements in the Northern Hemisphere and an underrepresentation of other regions such as tropical agroecosystems (Bouwman et al., 2002). Airborne data sets are beginning to become available (e.g., Nowak et al., 2010; Leen et al., 2013) and provide information about the vertical distribution of NH_3. It is worth noting that a few ship campaigns (e.g., Norman and Leck, 2005; Sharma et al., 2012) have also supplied NH_3 observations in oceanic atmosphere and that on-road measurements have recently been performed at landscape scale (Sun et al., 2014). The measurement gap identified above is of special importance considering the large variability of NH_3 in time and space.

Over the last few years satellite instruments able to detect NH_3 have begun to fill this observational gap, allowing new insights on global emissions, distributions and transport (Clarisse et al., 2009; Shephard et al., 2011; Van Damme et al., 2014a). Moreover, the spatial footprint of the satellite sounders currently available offers area-averaged measurements that are in much better correspondence with the grid cell size of current atmospheric chemistry and transport models in comparison to the point monitoring of atmospheric concentrations made at the ground (Flechard et al., 2013). First comparisons of model results with satellite measurements at global (Clarisse et al., 2009; Shephard et al., 2011) and continental (Heald et al., 2012; Van Damme et al., 2014b) scales have been achieved and suggest an underestimation of the modeled concentrations. Satellite sounders with a high spatio-temporal resolution, such as the Infrared Atmospheric Sounding Interferometer (IASI) or the Cross-track Infrared Sounder (CrIS; Shephard and Cady-Pereira, 2014), also offer the opportunity to identify area-specific and time-dependent emission profiles (Van Damme et al., 2014b). This would improve models that currently use a generalized and simplistic representation of the timing of emissions (van Pul et al., 2009). Satellite data are also being used in inversion methods (e.g., Zhu et al., 2013) to evaluate emission inventories at various scales (Streets et al., 2013).

While NH_3 satellite measurements have started to be used by models, their validation has yet to be performed even if sparse comparisons have already shown their consistency (e.g., Pinder et al., 2011; Shephard and Cady-Pereira, 2014). We present here the first attempt to validate IASI-NH_3 measurements with correlative data from the ground- and airplane-based measurements. We discuss these results crit-

ically (Sect. 3) considering the important mistime and misdistance errors (Wendt et al., 2013), which are introduced by comparing measurements of a very reactive species that are not perfectly collocated in time and space. In the next section we detail the IASI retrieval scheme implemented to derive NH_3 concentrations as well as the ground-based and airborne measurements used in this study.

2 Measurement data sets

2.1 Satellite observations

NH_3 was first detected in IASI spectra inside fire plumes above Greece in 2007 (Coheur et al., 2009). Subsequently, the development of a simplified retrieval method allowed the first global map of NH_3 from IASI observations to be produced (Clarisse et al., 2009). In Clarisse et al. (2010), a sensitivity study was performed, showing the abilities of infrared sensors to probe the lower troposphere, depending on atmospheric parameters such as the thermal contrast (see below). Recently, an improved IASI-NH_3 data set has been generated, combining better sensitivity and error characterization. The algorithm used to retrieve NH_3 columns from the radiance spectra is described in detail and compared to previous algorithms by Van Damme et al. (2014a). In short, the improved retrieval scheme exploits the hyperspectral characteristic of IASI and a broad spectral range between 800 and 1200 cm^{-1}. The algorithm consists of two steps. The first is the calculation of the hyperspectral range index (HRI), a dimensionless spectral index, from IASI Level 1C radiance. This HRI is converted in a second step to a total column of NH_3 using look-up tables (LUTs) built from forward radiative transfer model simulations under various atmospheric conditions. As the thermal contrast (temperature difference between the Earth's surface and the atmosphere at 1.5 km) is the critical parameter for infrared remote sensing in the lower troposphere, it is explicitly accounted for in the LUTs. Its value is derived from the temperature profile and surface temperature from the IASI Level 2 information provided by the operational IASI processor (August et al., 2012). The retrieval processing also includes an error estimate on the IASI-NH_3 total columns, taking into account the sensitivity of the satellite measurements to NH_3. This error estimate is especially important for comparisons with independent data sets (Van Damme et al., 2014b).

A known limitation of the retrieval method is that it uses only two fixed NH_3 profiles for the forward simulations (Fig. 3 in Van Damme et al., 2014a). The GEOS-Chem model was used to derive a source profile above land and a transported profile over oceans. The bias introduced by the use of these fixed profile shapes to build the LUTs for the total column retrieval is expected to be no higher than a factor of 2 on the total column values in the large majority of cases (Van Damme et al., 2014a). As independent total column data sets are not available and as the IASI-NH_3 measurements do not provide vertical information, these two modeled profiles are used in this paper to convert the retrieved column to a concentration at the surface and/or at an altitude of interest for the comparison with correlative data.

The IASI instrument is on board the polar sun-synchronous MetOp platform, which crosses the equator at a mean local solar time of 9.30 a.m. and p.m. It therefore allows global retrievals of NH_3 twice a day (Clerbaux et al., 2009). In this study, we only consider the measurements from the morning overpass as they are generally more sensitive to NH_3 because of higher thermal contrast at this time of day (Van Damme et al., 2014a). Given the high spatial variability of NH_3 concentrations, the footprint of the satellite measurement is an important parameter to take into account in comparing the retrieved columns with local ground-based measurements. IASI has an elliptical footprint of 12 km by 12 km (at nadir) and up to 20 km by 39 km (off nadir), depending on the satellite viewing angle. The availability of measurements is mainly driven by the cloud coverage as only the observations with a cloud coverage lower than 25 % are processed. Van Damme et al. (2014b) have shown, given the strong dependence on thermal contrast, that spring–summer months are better suited to accurately measure NH_3 from IASI (error below 50 %). The detection limit of NH_3 depends on both thermal contrast and the vertical distribution of NH_3; an illustration of this can be found in Fig. 5 of Van Damme et al. (2014a). As an example of detection limits on individual observation, a NH_3-retrieved column is considered detectable when the column is above 9.68×10^{15} molec cm^{-2} (1.74 µg m^{-3}) given a thermal contrast of 20 K, while the column should be larger than 1.69×10^{16} molec cm^{-2} (3.05 µg m^{-3}) for 10 K. Note that, due to the combination of high temporal and spatial variability of this trace gas, IASI-NH_3 observations are characterized by a high coefficient of variation: 187.8 % (for measurements with a relative error below 100 %) and 85.6 % (error below 50 %) for the morning measurements above land in 2011.

2.2 Ground-based observations

Monitoring NH_3 from the ground is not straightforward due to technical limitations and to high variability of concentrations in time and space (von Bobrutzki et al., 2010; Hertel et al., 2012). While the availability of NH_3 concentration and flux measurements at sub-landscape scales is increasing, measurements at landscape to regional scale are sparser (Flechard et al., 2013). In this study we use surface measurements from the US Ammonia Monitoring Network (AMoN, nadp.sws.uiuc.edu/amon/), the European Monitoring and Evaluation Programme (EMEP) network (nilu.no/projects/ccc/emepdata), the NitroEurope (NEU) Integrated project (nitroeurope.eu), the Netherlands National Air Quality Monitoring Network (LML, lml.rivm.nl), the IGAC/DEBITS/AFRICA (IDAF) network (idaf.sedoo.fr)

Table 1. Data sets used to compare with IASI satellite observations.

Network	No. of sites	Technique	Resolution	Location	Period used
AMoN	28	Passive diffusion-type sampler	2 weeks	USA	2011
EMEP	27	Various	Monthly	Europe	2011
IDAF	10	IDAF passive sampler	Monthly	Africa	2008 to 2011
NEU	53	DELTA systems	Monthly	Europe	2008 to 2010
NNDMN	43	DELTA systems and ALPHA passive sampler	Monthly	China	2009 to 2013*
LML	8	Annular denuder systems	Hourly	Netherlands	2008 to 2012

* All 2008 as well as January and February 2014 has been added for the Shangzhuang time series of Fig. 4.

and a series of observations from the Chinese Nationwide Nitrogen Deposition Monitoring Network (NNDMN, made available on request by X. Liu, China Agricultural University). The AMoN and EMEP data sets are used for the global comparison, the NEU and LML data sets are used for the regional assessment, while NNDMN and IDAF observations are used for both. These networks and their respective characteristics are summarized in Table 1. Additional details are provided below.

The EMEP network has been running since the 1980s, with data provided by the countries as part of the Convention on Long-Range Transboundary Air Pollution. These data are made available after national and EMEP quality assessments have been conducted (EMEP, 2014). For this analysis data from 27 sites were used, which have been generated from various national networks contributing to EMEP, so that instrumentation differs from one site to another (EBAS, 2014). The AMoN network was established in 2010 in the USA to monitor NH_3 with Radiello passive diffusion-type samplers (with a time resolution of 2 weeks) (NADP-National Atmospheric Deposition Program, 2012). From this network, we use the 28 sites which have started to provide measurements no later than 1 March 2011.

The NEU data set was generated using DELTA (DEnuder for Long-Term Atmospheric sampling) systems, detailed in Sutton et al. (2001). The network, which focused on Europe in the framework of the NEU Integrated project, is extensively described in Sutton et al. (2007) and Tang et al. (2009). Much effort was dedicated to providing a consistent data set with a high level of comparability (as the measurements were performed by different groups), including an inter-comparison study (Tang et al., 2009). It is worth noting that the precision for monthly means of a clean site using DELTA systems has been reported as below 10 % (Sutton et al., 2001). We use in our analyses the observations of 53 sites from 2008, 2009 and 2010 (Flechard et al., 2011). The Piana del Sele site was excluded as it is known to be unrepresentative for the area due to agricultural activities close by. The IDAF network is one of the few networks providing measurements not only for tropical agroecosystems but also for the whole Southern Hemisphere. It uses passive samplers (Ferm, 1991) which have been validated in situ and are associated with a reproducibility of 14.6 % (IDAF, 2014). Measurements at the 10 IDAF sites have been considered. The data used here for 2008–2011 show a similar annual cycle with comparable amplitudes to the data from the same network covering 1998 to 2007 presented by Adon et al. (2010). The NNDMN data set for China was generated using both DELTA systems (31 sites) and ALPHA (Adapted Low-cost, Passive High Absorption) samplers (12 sites) according to the methodology of Sutton et al. (2001) and Tang et al. (2001), as detailed for this network in Liu et al. (2011). The network mainly covered farmland sites but also included several grassland (two) and forest (four) sites across China.

Lastly, the LML network was operated using continuous annular denuder systems for the period considered here (1 January 2008–31 December 2012), based on the methodology of Wyers et al. (1993), although a switch to mini-Differential Optical Absorption Spectroscopy (miniDOAS) systems is planned for the near future in order to reduce running costs (Volten et al., 2012). The instrumentation used for this subset is characterized by a precision of 11 % (Wyers et al., 1993). It provides hourly NH_3 measurements at eight sites representative for the Netherlands since 1992 (Nguyen and R. Hoogerbrugge, 2009).

2.3 Airborne observations

Airborne measurements offer the advantage of providing concentrations at various altitudes and typically covering a surface area that is more representative of the satellite footprint than single ground-based observations. As NH_3 emissions result primarily from ground-based sources, measurements at higher altitudes are also characterized by less spatial variability, allowing improved comparison with satellite columns. Aircraft observations are able to capture, to some extent, the intra-footprint variability spread in situ which is integrated in each satellite observation. By comparison, aircraft observations of NH_3 typically focus on short-term campaign measurements.

The airborne data set used for this analysis was collected during the CalNex campaign (California Research at the Nexus of Air Quality and Climate Change), which took place in May and June 2010 in California, USA (Ryerson et al., 2013; Parrish, 2014). NH_3 was measured by chemi-

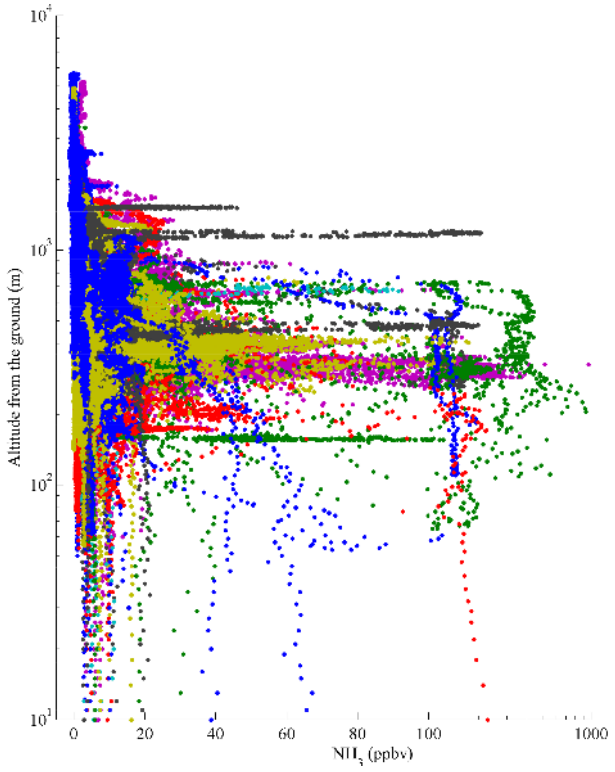

Figure 1. Vertical distribution of NH_3 airborne measurements from the NOAA WP-3D flights during the CalNex campaign in California (2010). Each color corresponds to 1 day of measurement.

cal ionization mass spectrometry (CIMS, uncertainty of $\pm$ (30 % + 0.2 ppbv)) during 16 flights of the National Oceanic and Atmospheric Administration (NOAA) WP-3D aircraft (Nowak et al., 2007, 2010, 2012). The observations were made at 1 Hz which is equivalent to 100 m spatial resolution, with the majority of measurements at altitudes from 10 m to 2 km above ground. Nowak et al. (2012) used this data set to show the underestimation of NH_3 emissions from dairy farms and automobiles in regional emissions inventories and to assess the impact of these sources on the formation of ammonium nitrate. Figure 1 presents the high-resolution NH_3 profiles from the campaign, with x axis being linear from 0 to 100 pbbv and logarithmic from 100 to 1000 ppbv. The large majority of measurements range from 0 to 100 ppbv, with few measurements reaching as high as several hundred ppbv.

3 Results and discussions

This section starts with a comparison between IASI-NH_3 observations and ground-based measurements. A first qualitative NH_3 global comparison is performed for the year 2011, followed by quantitative regional analyses with data sets over Europe, China and Africa. Then the ground-based hourly measurements provided by the Dutch national network (LML) are used to evaluate the IASI measurements collocated in time and to discuss the challenges of validating the satellite measurements of reactive species, showing high spatial and temporal variability. The added value of the airplane measurements for validation of IASI-NH_3 measurements is presented in Sect. 3.2.

3.1 Comparison with ground-based observations

3.1.1 Global evaluation

Figure 2 shows the NH_3 distribution measured by IASI for 2011 and gridded at 0.25° lat × 0.5° long resolution for the areas covered by the available measurement data sets. In this graphic a weighting procedure has been applied on the IASI daily columns to take into account the error variability of the data set within the average (Van Damme et al., 2014a). The main agricultural source areas are observed in the Indo-Gangetic plain, the North China Plain (NCP) as well as intensive agricultural valleys such as the Ferghana Valley in central Asia and the San Joaquin Valley in California (Clarisse et al., 2009, 2010). High NH_3 values are also seen over burned areas mainly in Eastern Europe (April) (IFFN-GFMC-16, 2011), over the Magadan region in eastern Russia (May and especially second part of July) (NASA, 2011) and in Indonesia (March). Ground-based data sets of NH_3 concentrations for 2011 have been superimposed in Fig. 2. What is striking from the collected data sets for that year is the scarcity of the NH_3 measurements in some parts of the world. Except for the IDAF stations in Africa, no measurements were available for 2011 in the rest of the tropical region and in the Southern Hemisphere. Nevertheless, we find a broadly similar pattern in the surface measurement as in the satellite-derived distribution, with the largest concentrations for the Chinese stations, followed by the IDAF sites in Africa. Europe and the USA present lower concentrations with the exception of the Eibergen station (EMEP) in the Netherlands (see also below).

Although the comparison with the IASI measurements is qualitatively reasonable, we find that in North America the satellite-retrieved columns are relatively higher than the ones reported by the AMoN network. It is worth noting that the sites with yearly concentrations available for 2011 are mainly located outside the intensive source areas for the USA. In China, the highest values are observed (from the ground and IASI) in the NCP and in the Chengdu Plain (Sichuan basin). The satellite columns are lower in southeastern China, which is consistent with the high-resolution NH_3 emissions inventory from Huang et al. (2012). In Europe, the EMEP stations are mainly located in its central part, where IASI-NH_3 columns have low values, in agreement with the ground-based concentrations. The Netherlands is the principal hotspot region in the northern part of central Europe in both the satellite and surface measurements. A second

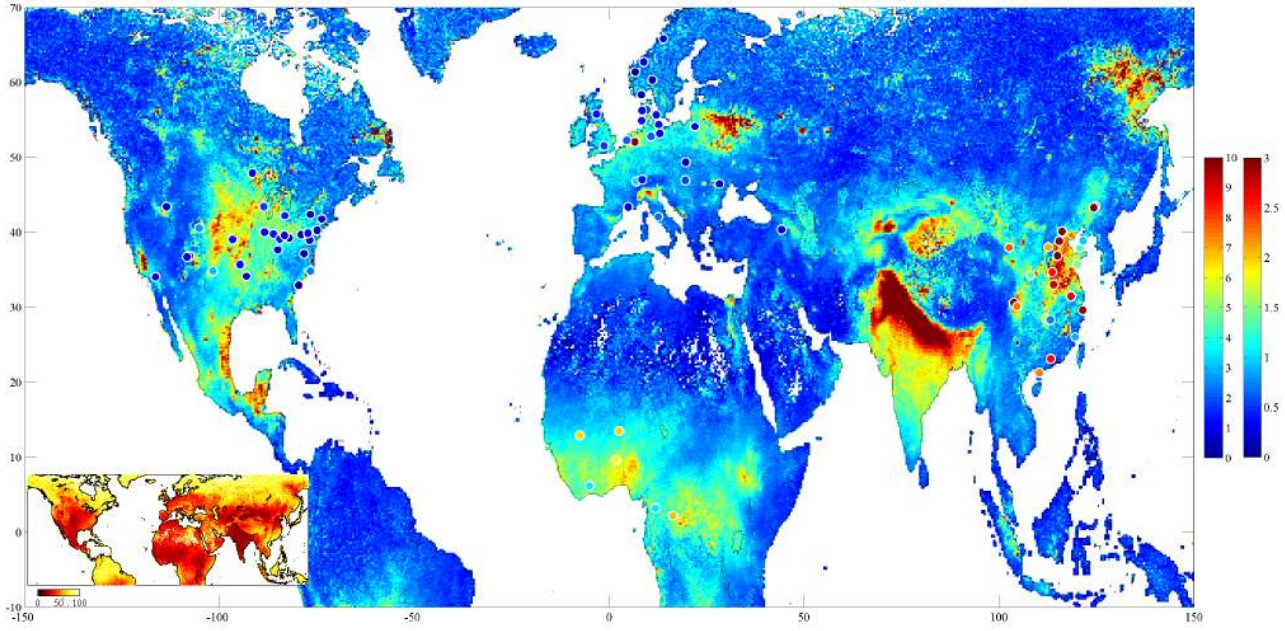

Figure 2. Yearly averaged surface concentrations ($\mu g\,m^{-3}$, left vertical color bar) from IDAF, AMoN, EMEP and NNDMN data sets plotted on top of the NH_3 IASI satellite column ($\times 10^{16}$ molec cm^{-2}, right vertical color bar) distribution for 2011 gridded at 0.25° lat × 0.5° long. Columns and relative error (%, bottom left inset) have been calculated as a weighted mean of all IASI measurements within a cell, following equations described in Van Damme et al. (2014a) (columns with an associated relative above 100 % have been filtered).

hotspot in Europe is the Po Valley of northern Italy. Although this was not represented by the EMEP measurements, this is subject of a specific analysis under the ECLAIRE project (eclaire-fp7.eu).

3.1.2 Regional focus

Monthly resolved data sets

Figure 3 presents a similar comparison with focus over Europe (left), China (middle) and Africa (right). The top panels show the IASI-retrieved column distributions ($\times 10^{16}$ molec cm^{-2}, right vertical color bar) on which the ground-based concentrations from the NEU and the NNDMN network ($\mu g\,m^{-3}$, left vertical color bar) and the volume mixing ratio (VMR) from the IDAF network (ppbv, left vertical color bar) have been superimposed. The bottom panels provide the corresponding correlation plots with their linear regression fits (reduced major axis), and Pearson's correlation coefficient (r, underlined when significant). For this comparison the IASI columns have been converted to surface concentrations by using the model profiles considered in the retrieval procedure (Van Damme et al., 2014a). Although such a conversion introduces additional errors, it allows direct comparison with similar quantities. We note that while the conversion to surface observation does not change the correlation much, it determines the intercept. The use of an inadequate profile shape leads unavoidably to biased surface concentrations from IASI. As an example, the Pearson's r calculated when comparing IASI total columns and NEU ground-based concentrations is equal to 0.284, while it is equal to 0.275 when comparing satellite and ground-based surface concentrations.

For Europe, the averaged satellite distribution for 2008, 2009 and 2010 is presented with superimposed the 3-year mean NEU ground-based observations (Fig. 3, top left). High values can in particular be seen in the western part of Russia, which is an area that was strongly impacted by the Russian fires of 2010 (R'Honi et al., 2013). The effect of these fires appears to be overrepresented in the satellite distribution due to the weighted averaging procedure associated with the higher IASI sensitivity in fire plumes (Van Damme et al., 2014a, b). However, overall IASI observes a similar pattern as that reported by the NEU sites. The highest surface concentrations are measured in northwestern Europe, going up to 7 $\mu g\,m^{-3}$ at Cabauw, Netherlands, where satellite columns are above 2×10^{16} molec cm^{-2}. The lowest surface concentrations reported by the NEU network are observed at the northern European stations, where IASI columns are low too. The statistical analysis (Fig. 3, bottom left) gives a significant correlation. This is especially true considering that we are comparing monthly averaged surface concentrations from ground-based instruments (integrated over day and night) with the monthly satellite mean that includes only measurements from the morning overpass time (only monthly means with an IASI-weighted relative retrieval error below 100 % have been taken into account). The linear regression is indi-

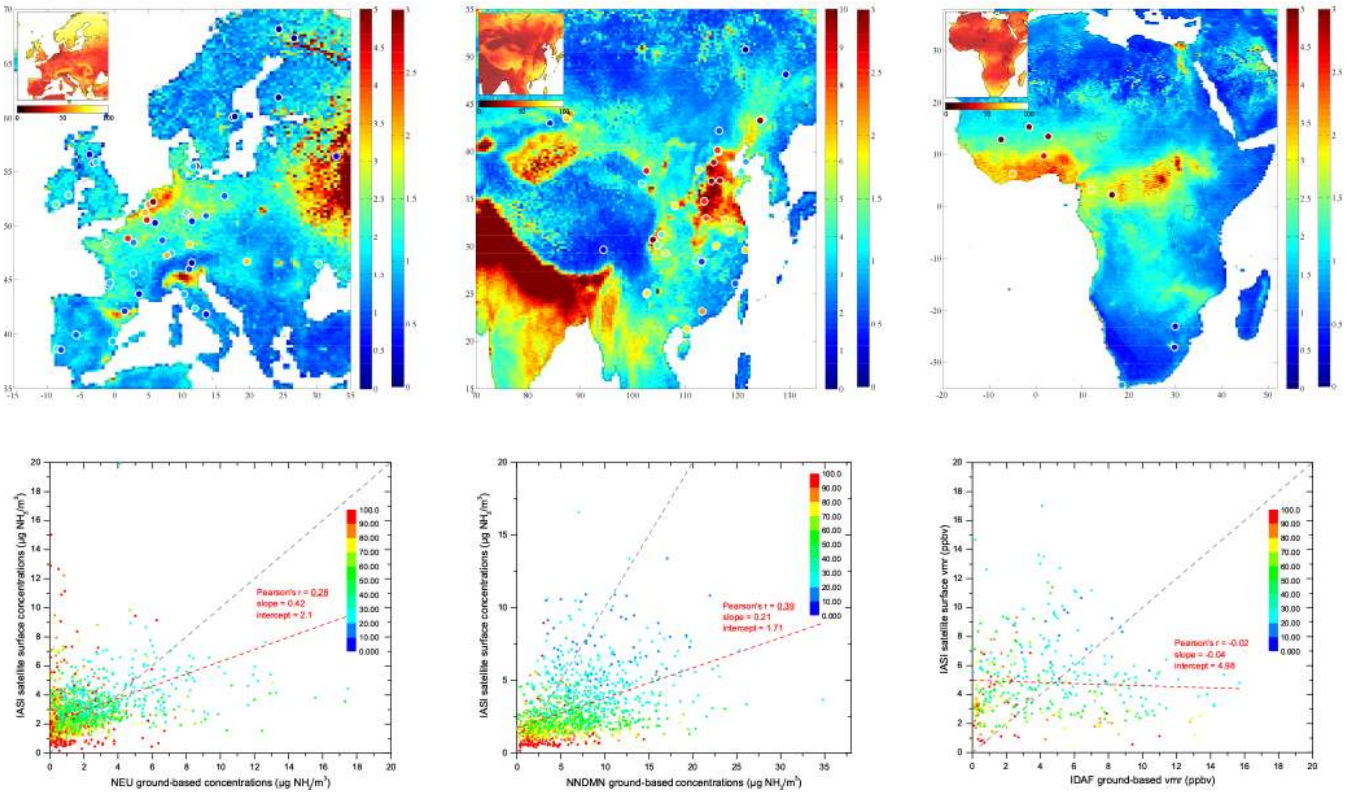

Figure 3. Top: ground-based quantities (left vertical color bar) from NEU (μg m^{-3}, left panel), NNDMN (μg m^{-3}, middle panel) and IDAF (ppbv, right panel) data sets plotted on top of the NH_3 satellite columns ($\times 10^{16}$ molec cm^{-2}, right vertical color bar) distribution gridded at 0.25° lat × 0.5° long, both averaged for the period covered by the data sets. Stations with less than two-thirds of measurement availability for the period considered have been excluded. The relative error distribution from IASI retrieval is shown as inset (top left, %, horizontal color bar). Columns/errors have been calculated as a mean of all the measurements within a cell, weighted by the relative error following equations described in Van Damme et al. (2014a). Bottom: monthly NEU (left panel), NNDMN (middle panel) ground-based concentrations (μg m^{-3}) and IDAF (right panel) ground-based VMR (ppbv) vs. IASI-retrieved NH_3 surface concentrations (μg m^{-3}) or VMR (ppbv). The color scale corresponds to the IASI retrieval errors (%). Dashed red lines represent the linear regression and gray dashed lines represent the one-to-one line. The Pearson's r (underlined when significant (p value below 0.05)), slope and intercept are also indicated in red.

cated in red and is characterized by a Pearson's r of 0.28 (n = 1337 number of coincidences), a slope of 0.42 and an intercept at 2.1 μg m^{-3}. Note that if the satellite data are restricted to the monthly mean concentrations with associated error below 75 %, the Pearson's r increases to 0.35 ($n = 961$). Almost all the sites in Europe are characterized by a positive correlation coefficient when it is significant (p value below 0.05). The highest correlation ($r = 0.81$) is obtained for the Fyodorovskoye site (RU-Fyo), and this is explained by the very large columns observed during the Russian fire event of 2010. The second site characterized by a high correlation coefficient is the Monte Bondone site (IT-MBo) with $r = 0.71$, which is characterized by high NH_3 concentrations in summer and low in winter, consistent with local livestock grazing patterns. By contrast, the most northern sites (located in Finland) indicate a negative correlation (Hyytiälä, $r = -0.44$; Lompolojänkkä, $r = -0.43$; Sodankylä, $r = -0.45$) with an associated p value slightly above 0.05. These are the sites with very low ground level concentrations (3-year average close to 0.1 μg m^{-3}), suggesting that the monthly variability for such small concentrations in a region associated with low thermal contrast cannot be reliably detected by IASI. The other NEU stations with a significant r above 0.5 include Brasschaat (BE-Bra, 0.54), Fougères (FR-Fou, 0.58) and Vall d'Alinyà (ES-VDA, 0.58). The list of stations and their respective correlation coefficient, as well as their associated p and n values, is provided in Table A1.

For China (2009 to 2013), the spatial patterns in NH_3 abundance are in good agreement (Fig. 3, top middle panel). We find the highest concentrations in the NCP area and the lowest in remote areas such as the Linzhi site (LZ, on the Tibetan Plateau) and several sites in northeast China. To better illustrate the potential for a high degree of correspondence between the satellite columns and the surface measurements, we provide in Fig. 4 the monthly averaged time series at Shangzhuang (SZ) from the ground and from space ($r = 0.72$). This suburban station northwest of Beijing (40.14° N, 116.18° E), surrounded by agriculture and far

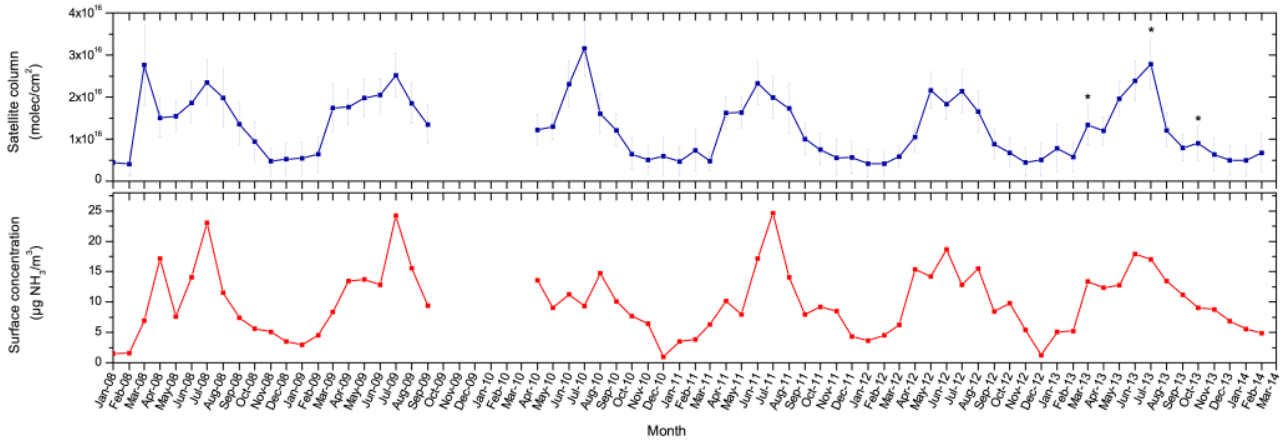

Figure 4. Time series of monthly averaged NH_3 satellite columns (top, blue, molec cm^{-2}) and ground-based concentrations (bottom, red, $\mu g\,m^{-3}$) at Shangzhuang site (40.14° N, 116.18° E) in the North China Plain (NCP) from January 2008 to February 2014. The associated weighted mean error for each month is calculated following equations described in Van Damme et al. (2014a) and presented here as error bars. Asterisks highlight the fertilization peaks of March, July and October 2013 (Shen et al., 2011).

from a main road (Shen et al., 2011), has one of the longest records of NH_3 concentrations in China, from January 2008 to February 2014. The IASI-derived total columns (top, blue, molec cm^{-2}) reproduce nicely the ground-based concentrations (bottom, red, $\mu g\,m^{-3}$) time evolution with concentration peaks in summer (June–July), close to 25 $\mu g\,m^{-3}$ at the surface and around 3×10^{16} molec cm^{-2} observed from IASI. Looking at interannual variability, for example in 2013, the fertilization peaks of March, July and October are clearly observed (Shen et al., 2011). It is interesting to note that the highest January surface concentration (5.1 $\mu g\,m^{-3}$) and satellite total column (7.8×10^{15} molec cm^{-2}) are measured during the severe winter pollution episode of 2013 (see Boynard et al., 2014; Wang et al., 2014). The correlation analysis for the monthly values of the 43 NNDMN sites gives a Pearson's r equal to 0.39 (considering the IASI data with a monthly relative retrieval error below 100 %) and a slope of the regression equal to 0.21 ($n = 1149$). The Pearson's r is globally higher than for Europe probably due to the higher concentrations in China. This is also observed in the monthly retrieval error which are overall lower. In addition to Shangzhuang, the sites with a significant Pearson's r above 0.5 are China Agricultural University (CAU, 0.51), Lingshandao (LSD, 0.55), Changdao (CD, 0.58), Gongzhuling (GZL, 0.52), Bayinbuluke (BYBLK, 0.59), Fengyang (FY, 0.64), Ziyang (ZY, 0.58), Yanting (YT, 0.70) and Dianchi (DC, 0.64), where the p values for these sites are all less than 0.01. Only one site in the NNDMN network gives a significant negative correlation: the cleanest site in the network in Tibetan Plateau (LZ, $r = -0.75$). With a mean ground-based concentration of 1.03 $\mu g\,m^{-3}$, this again illustrates, as suggested with the Finnish sites, the limitation of IASI to provide reliable monthly NH_3 values at very low concentrations. The results for all the sites are presented in Table A2.

For Africa, both IASI and surface network report the highest values in western and central Africa and the lowest in South Africa for the 4-year average (2008 to 2011, Fig. 3 top right panel). However, over Western Africa the highest VMR are reported by the network for the dry savanna sites (located above 10° N), while IASI observes higher columns closer to the coast. This could possibly be due to the lack of IASI sampling above these Sahelian sites during the rainy season in June–July, which is characterized by large concentrations measured at the surface. The high density of livestock concentrated on the fresh pasture at that time implies high surface emissions. However, this time period is typically also associated with a high deposition and/or cloud coverage, preventing IASI from capturing these events while they are monitored from the ground (Adon et al., 2010). Adon et al. (2010) have shown that the dry savanna sites are characterized by higher concentrations during the wet season (June–July); conversely, the wet savanna sites (closer to the West African coast) present the larger amount during the dry season (January–February). The latter may therefore be better monitored by IASI. The right bottom plot (Fig. 3) compares the surface VMR for Africa in ppbv. There is no correlation when the data of all the sites are grouped. This could be explained by the sparsity of the IDAF data set combined with the difficulties of the satellite to catch specific high emission events. The only station showing a positive significant Pearson's r is Lamto (Ivory Coast, 0.39), which is not surprisingly a wet savanna site. The comparison for each station individually is provided in Table A3.

In general, the regression intercept is relatively high, while the slope is relatively low. For all three regions the largest measured concentrations are underestimated in the IASI surface-derived data. This smaller range of concentrations could be a consequence of using a fixed vertical profile shape

Table 2. Statistical analysis of the comparison of LML and IASI satellite surface concentrations in the Netherlands from 1 January 2008 to 31 December 2012. The spatial averaging (two bottom rows in the table) consists of considering the mean of all the ground-based observations and the mean of the satellite observations in the area covered by the LML network (considered here as the box 51.185–53.022° N and 4.01–7.106° E). The temporal averaging (bottom row) consists in taking the mean of the observations (at the overpass time of the satellite) on a monthly basis. The slope and the intercept of the linear regression are indicated by a and b while the significant Pearson's correlation coefficients (r) are underlined (p value below 0.05); n corresponds to the number of points. Only IASI-derived values with a relative retrieval error below 100 % have been taken into account.

Site (lat–long)	a	b	r	n
Vredepeel (51.541° N–5.854° E)	0.04	2.49	0.16	94
Huijbergen (51.435° N–4.360° E)	0.3	1.08	0.31	54
De Zilk (52.298° N–4.510° E)	0.16	0.89	0.39	45
Wieringerwerf (52.805° N–5.051° E)	0.03	1.26	0.11	91
Zegveld (52.139° N–4.838° E)	0.07	1.38	0.21	93
Eibergen (52.096° N–6.606° E)	0.12	1.46	0.38	102
Wekerom (52.113° N–5.709° E)	0.03	1.91	0.25	87
Valthermond (52.877° N–6.931° E)	0.63	−1.39	0.49	78
All sites individually	0.07	1.68	0.29	644
All sites spatially averaged	0.21	0.96	0.28	960
All sites spatially and temporally averaged	0.19	1.86	0.47	58

in the retrieval procedure for IASI spectra. Indeed, in the case of a low boundary layer height, concentrations are larger in that narrow layer, which is not considered by the straightforward procedure applied to retrieve IASI surface concentrations from the columns. Moreover, the vertical profiles above land from the GEOS-Chem model have already been identified as being too low above California, especially for strongly polluted areas (Schiferl et al., 2014). Another reason could lie in the influence of very local sources on the ground-based data (see further). Contrary to what we find for high concentrations, there is a positive bias of IASI for low concentrations. There are at least three possible reasons for this. The first stems from the way the relative retrieval errors are taken into account. Applying weighted averaging of IASI columns using the relative retrieval error tends to favor the largest concentrations, as the lower values are associated with higher error estimates for the same value of thermal contrast (Van Damme et al., 2014a). A second reason, in the case of very low NH_3 amounts, is that the random error of the HRI always translates into a positive contribution of the column (and hence does not average to zero for zero NH_3). The third reason is again linked with a misrepresentation of NH_3 vertical distribution. In low NH_3 abundance cases and/or in areas where NH_3 is being deposited, there is no strong vertical gradient near the surface. The use of a polluted profile shape (peaking at the surface) in the retrieval procedure of IASI surface concentrations tends to overestimate the surface contribution of the total columns.

We recall that all regressions shown and discussed in this section are based on weighted monthly IASI-derived NH_3 means, with the weight being determined by the relative error of the individual retrieved columns. We also made the comparisons with unweighted monthly means and found somewhat different parameters for the regression line but an overall weak impact on the regression coefficients. In all cases, the slope remains well below 0.5 and the intercept smaller but still positive.

Hourly resolved data set

The LML data set offers long-term hourly resolved NH_3 measurements allowing the investigation of individual IASI observations and testing the effect of averaging different time scales. However, it is worth noting that this network provides measurements in an area (the Netherlands) that is not particularly favorable for infrared remote sensing of surface pollution (low thermal contrast and relatively high cloud coverage). Table 2 summarizes the results from the comparison of the IASI concentrations (columns converted to surface concentrations as above) to those measured from the ground. The upper part presents the comparison from the linear regression for each individual site (slope (a) and intercept (b) of the linear regression, Pearson's r (underlined when significant) and the number of observations (n)). We took into account only the IASI measurements covering the stations, which means that the true elliptical footprint is considered and only the observations including the LML site are kept. Six of the sites show significant correlation and for all, except for one (Valthermond, which has a negative intercept and fairly high slope), we find a very low slope (0.03–0.3) but a high intercept between 0.89 $\mu g\,m^{-3}$ (De Zilk) and 1.91 (Wekerom). This shows again the difficulties of IASI to capture the entire range of local surface concentrations, as explained above. The best Pearson's r are observed for Valther-

mond (0.49), De Zilk (0.39) and Eibergen (0.38) sites. When all the sites are taken together we obtain a Pearson's r of 0.29, a slope of 0.07 and an intercept of 1.68 µg m^{-3}. These results, obtained by comparing individual IASI value with ground-based measurement at the overpass time of the satellite, could be due, as discussed previously, to the misrepresentation of the vertical distribution in the processing of the spectra and the need to consider the boundary layer height.

A factor preventing one from drawing strong conclusions from this comparison is the spatial representativity of the ground-based measurement within the large footprint of the satellite (going from 113 km^2 at nadir to around 613 km^2 for the highest satellite viewing angles). It means that local sources inside the satellite footprint could have a strong influence on the IASI column values but not be represented in the ground-based data sets due to the high horizontal gradient of NH_3 concentrations around the source (Fowler et al., 1998; Sutton et al., 1998; Hertel et al., 2012). Conversely, background concentrations within the IASI pixel will tend to mask single local sources. The representation issue of ground-based measurement stations has already been highlighted during model performance evaluation (Wichink Kruit et al., 2012). To avoid this uncertainty, which is difficult to assess in the validation, we could consider the general rule that the LML network is representative for the entire Netherlands (Nguyen and R. Hoogerbrugge, 2009). For instance, using the eight stations together we can calculate a daily mean concentration of NH_3 at the overpass time of the satellite that we compare with the IASI-weighted mean of the measurements inside the area covered by the network (considered here as the following box: 51.185–53.022° N and 4.01–7.106° E). Doing so, we find that the Pearson's r increases to 0.28, while the slope and the intercept of the linear regression are 0.21 and 0.96 µg m^{-3}, respectively.

Finally, to investigate the impact of temporal variability and to compare with the previous results of monthly resolved data, we calculated monthly average of IASI measurements above the Netherlands and the LML ground-based concentrations at the IASI overpass time. The time series of Fig. 5 show the temporal variability in 2008, 2009, 2010, 2011 and 2012 of IASI-NH_3 columns (top panel, blue, molec cm^{-2}) and of the surface concentrations derived from IASI columns (bottom panel, red, µg m^{-3}) and monitored by the LML sites (bottom panel, black, µg m^{-3}). Only values with a relative retrieval error below 100 % have been taken into account. The spring peak linked with fertilization practices in the Netherlands is clearly identifiable in the LML and IASI time series in March/April. Looking at the surface concentrations, a fair agreement is found between the ground-based and the satellite observations. The monthly variability is consistent between both instruments even if the IASI-derived values are not reproducing with the same amplitude the peaks observed from the ground. This could be due, as explained previously, to a misrepresentation of the NH_3 vertical distribution. As shown in the lowest row of Table 2, the comparison based

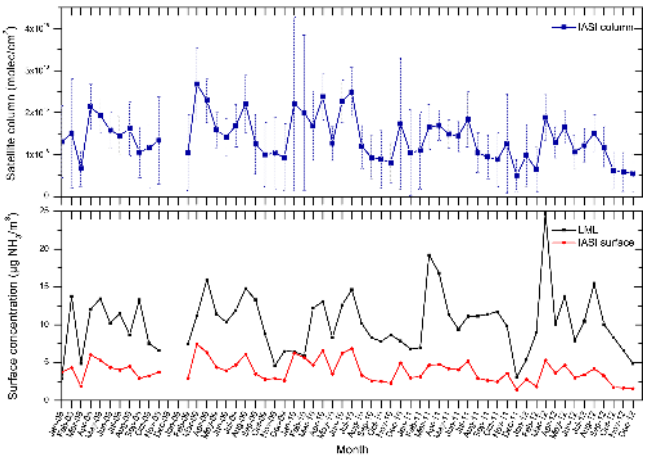

Figure 5. Monthly time series of NH_3 satellite columns (top, blue, molec cm^{-2}) and surface concentrations at the overpass time of the satellite (bottom) from all the sites of the Dutch LML network averaged (black, µg m^{-3}) and from IASI satellite observations (red, µg m^{-3}) (in the box 51.185–53.022° N and 4.01–7.106° E, corresponding to the area covered by the Dutch network), covering 2008, 2009, 2010, 2011 and 2012. The associated error bars are based on the retrieval error for each monthly column, calculated following equations described in Van Damme et al. (2014a). Only monthly means associated with weighted relative retrieval errors below 100 % are shown.

on monthly data is characterized by a Pearson's r of 0.47, substantially higher than the ones obtained with the previous data sets. The linear regression has a slope of 0.19 and an intercept of 1.86 µg m^{-3}.

3.2 Comparison with airborne observations

California is an important NH_3 source area in the USA. Major sources include livestock operations, agricultural fertilizers, waste management facilities and motor vehicles (Parrish, 2014). Figure 6 presents the NH_3 distributions for the area and period covered by the CalNex campaign (from 30 April to 24 June 2010). The airborne distribution (top panel, ppbv) is consistent with the satellite one (bottom panel, $\times 10^{16}$ molec cm^{-2}). The retrieval error distribution is also presented as inset (bottom left of right panel, %). The pattern observed is characterized by the highest concentrations in the San Joaquin and Sacramento valleys, as well as in the South Coast Air Basin (SCAB). High concentrations are also measured in the Imperial Valley and to a lesser extent in the neighborhood of Phoenix. Note that the high values reported by the airborne measurements on 22 June above upper western part of Colorado are also measured by IASI.

To compare satellite observations with the CalNex data set, the IASI total columns are first converted to concentrations at the altitude of interest for each airborne measurement located inside the satellite footprint. The concentrations (airborne or satellite based) covering the footprint of IASI are

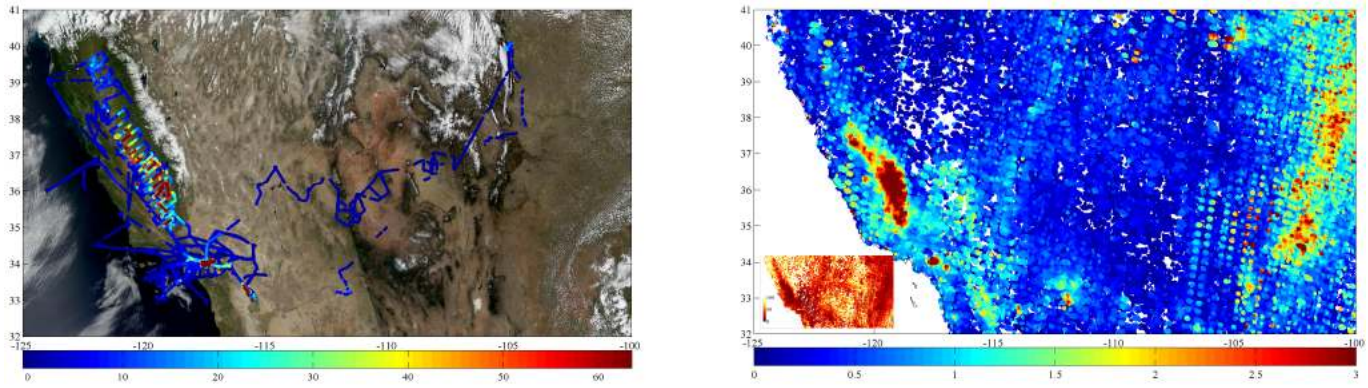

Figure 6. NH_3 distribution measured from CIMS instrument on-board NOAA WP-3D aircraft (left, ppbv) and IASI satellite (right, molec cm^{-2}) averaged for the flight period of the CalNex campaign (from 30 April 2010 to 24 June 2010). Averaged relative retrieval error (%) of the IASI-NH_3 columns are presented as inset in the lower left corner of right panel. Only column means associated with weighted relative retrieval errors below 100 % are shown.

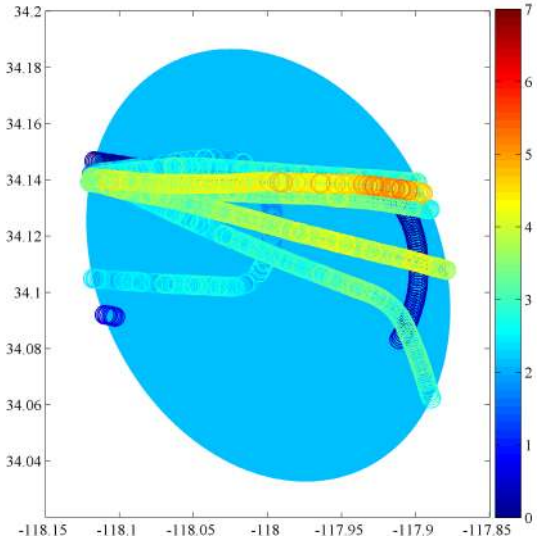

Figure 7. Spatial distribution of 1515 airborne observations made on-board the NOAA WP-3D aircraft at various altitudes superimposed on the corresponding IASI footprint. The color scale corresponds to the individual concentrations (ppbv) measured by the CIMS instrument, while the value for IASI is the average of the VMR calculated from the same total column at the different altitudes of the aircraft.

then averaged in a second step. This results in 222 corresponding pairs of observations to which we can apply thresholds on the mistime (being the time difference between the IASI overpass and the airborne measurement), the retrieval error or the number of airborne observations by IASI footprint.

As an illustration, Fig. 7 shows observations in the SCAB (satellite footprint centered at 34.12° N and 118° W) characterized by a satellite mean concentration of 2.17 ppbv (associated with a relative retrieval error of 25 %) and an airborne concentration of 2.65 ppbv. This subset of observations has been selected as the one with the highest density of airborne measurements for a given IASI footprint (with a relative retrieval error below 100 %) considering a mistime below 3 h. The IASI footprint in that case includes 1515 individual airborne observations spanning altitudes from 272 m to 2.6 km.

Table 3. Statistical analysis of the CalNex and IASI satellite vmr comparison. The slope (a) and the intercept (b) of the linear regressions are indicated for various criteria on the data selection, as well as their respective Pearson's correlation coefficients (r, in italic font when significant); n correspond to the number of pairs of observations.

Retrieval error	Mistime	a	b	r	n
No filter	No filter	0.07	2.31	*0.36*	222
No filter	< 3 h	0.18	0.64	*0.72*	75
< 100 %	< 3 h	0.18	0.49	*0.82*	70
< 100 %	< 1 h	0.17	0.13	*0.99*	15

The results obtained from the comparison are presented in Table 3. The first row gives the statistical parameters for all the coupled observations. This comparison is characterized by a Pearson's r of 0.36 ($n = 222$), a slope of 0.07 and an intercept at 2.33 ppbv. Only considering pairs of observations with a mistime of less than 3 h, the Pearson's r increases significantly to 0.72 ($n = 75$). If a threshold on the relative retrieval errors is also taken into account (in this case being < 100 %), the r increases further to 0.82. Finally, if we constrain the mistime to be lower than 1 h, the Pearson's r reaches 0.99 ($n = 15$). With increased filtering, a decrease of the intercept is also observed. However, it is notable that the slope of the regression does not change substantially, remaining at around 0.17 to 0.18, indicating underestimates of NH_3 in VMR compared to the aircraft measurements using CIMS.

4 Conclusions and perspectives for the validation

Overall, IASI satellite measurements of NH_3 are consistent with the available data sets used in this study. This paper presents only the first steps to validate IASI-NH_3 columns. As shown, it is not straightforward and depends strongly on data availability as well as on their representativity for satellite observations. The yearly distributions reveal consistent patterns and highlight the scarcity and the spatial heterogeneity of NH_3 observations from the ground, with very few measurements in the Southern Hemisphere and tropical agroecosystems. Comparisons with monthly resolved data sets in Europe, China and Africa have shown that IASI NH_3-derived concentrations are in fair agreement considering that the ground-based observations used here for comparison are mainly monthly integrated measurements, while the satellite monthly weighted means are only taking observations at the morning overpass time into account.

The comparison between IASI-derived concentrations and the surface concentrations measured locally was assessed using linear regressions. Statistically significant correlations were found at several sites, but low slopes and high intercepts were calculated in all cases. Overall, this points to a too-small range in the IASI surface concentrations, which could partly be due to the lack of representativity of the point surface measurements in the large IASI pixel. Another possible reason for the difference lies in the use of a simple profile shape in the retrieval procedure, which does not take into account variations in the boundary layer height and hence in the mixing of pollution close to the surface. As shown in previous studies, accounting for realistic boundary layer heights in the retrieval of tropospheric column from satellite measurements improves on the comparison with surface measurements (e.g., see Boersma et al., 2009). A third possible contributing reason for the large intercept and low slope is a bias in the IASI values derived from weighted averaging, where more weight is given to data with the least uncertainty. Under clean conditions, when there is a weak signal, this tends to give more weight to high values, which partly explain the high intercept values.

In addition to the comparison with ground-based measurements, this paper has also provided a comparison of the IASI-derived VMR to vertically resolved CIMS measurements from the NOAA WP-3D airplane during the CalNex campaign in 2010. The main advantage of such a comparison lies in the fact that numerous airborne measurements are available within the satellite footprint, strongly reducing spatial representativity issues. Moreover, airborne measurements are performed at altitudes that are more in line with the sensitivity of infrared nadir sounders. Consequently, a much higher correlation between IASI and the airplanes is found, e.g., characterized by a correlation coefficient of 0.82 for subset of observations associated with a retrieval error below 100 % for IASI and a mistime below 3 h. Low slopes and large intercept values from the linear regressions are nevertheless obtained, as they were with the ground-based measurements, further suggesting a poor representativity of the profile shape used for IASI retrievals for these high pollution regions.

More generally, this first attempt to validate the NH_3 measurements from IASI has highlighted known limitations in both the retrieval procedure (fixed vertical profile and boundary layer height) and in the correlative measurements, which are in many cases not representative of what the satellite measures horizontally and vertically. All statistical results were shown for concentrations (or VMR) and do not allow the validity of the IASI-derived columns to be assessed, which is – considering the limited vertical sensitivity achievable – the most relevant quantity available from these satellite measurements. Therefore, here we highlight the need to acquire more comprehensive data sets of NH_3 columns, e.g., by using boundary layer heights and NH_3 profile measurements (and/or estimates) to infer the columns abundance from the surface observations. For this purpose, dedicated measurement campaigns focusing on the NH_3 vertical profile or additional total column measurements from ground-based Fourier transform infrared, which are becoming available (Vigouroux et al., 2013), will no doubt allow improvements in the validation of NH_3 satellite-retrieved columns in the future.

Appendix A

Table A1. Statistical analysis of the NEU data set and monthly IASI satellite surface concentrations comparison for each stations during 2008, 2009 and 2010. Each site is characterized by its site code and name, coordinates, its Pearson's correlation coefficient (r) and the associated p value as well as its number of points (n). Only monthly values with a relative IASI retrieval errors below 100 % have been taken into account.

Site code	Site name	Lat (° N)	Long (° E)	r	p value	n
IT-Amp	Amplero	41.90	13.61	−0.26	0.50	9
UK-Amo	Auchencorth Moss	55.79	−3.24	0.08	0.67	33
FR-Bil	Bilos	44.52	−0.90	0.05	0.86	14
BE-Bra	Brasschaat	51.31	4.52	0.56	0.00	27
HU-Bug	Bugac	46.69	19.60	−0.12	0.51	34
NL-Ca1	Cabauw	51.97	4.93	0.40	0.02	35
IE-Ca2	Carlow	52.85	−6.90	0.02	0.92	31
IT-Col	Collelongo	41.85	13.59	−0.09	0.61	34
IE-Dri	Dripsey	51.99	−8.75	0.31	0.14	24
UK-ESa	East Saltoun	55.90	−2.84	−0.01	0.97	9
ES-ES1	El Saler	39.35	−0.32	−0.19	0.30	33
PT-Esp	Espirra	38.64	−8.60	0.31	0.07	34
FR-Fon	Fontainbleau	48.48	2.78	0.17	0.35	31
FR-Fou	Fougères	48.38	−1.18	0.58	0.00	24
RU-Fyo	Fyodorovskoye	56.46	32.92	0.81	0.00	27
DE-Geb	Gebesee	51.10	10.91	0.47	0.01	27
UK-Gri	Griffin	56.62	−3.80	−0.48	0.41	5
FR-Gri	Grignon	48.84	1.95	0.08	0.67	32
DE-Gri	Grillenburg	50.95	13.51	0.39	0.04	29
DE-Hai	Hainich	51.08	10.45	−0.03	0.89	28
FR-Hes	Hesse	48.67	7.07	0.12	0.55	28
DE-Hoe	Höglwald	48.30	11.10	−0.02	0.90	30
NL-Hor	Horstermeer	52.03	5.07	0.21	0.24	33
FI-Hyy	Hyytiälä	61.85	24.30	−0.44	0.05	21
DE-Kli	Klingenberg	50.89	13.52	−0.14	0.47	29
CH-Lae	Laegern	47.48	8.37	−0.04	0.81	31
FR-Lq2	Laqueuille	45.64	2.74	0.19	0.33	30
ES-LMa	Las Majadas	39.94	−5.77	0.22	0.21	34
FR-LBr	Le Bray	44.72	−0.77	0.50	0.14	10
FI-Lom	Lompolojänkkä	68.21	24.35	−0.43	0.10	16
BE-Lon	Lonzee	50.55	4.74	0.21	0.32	25
NL-Loo	Loobos	52.17	5.74	0.33	0.08	29
DE-Meh	Mehrstedt	51.28	10.66	0.26	0.20	25
PT-Mi1	Mitra II (Evora)	38.54	−8.00	−0.11	0.58	29
IT-MBo	Monte Boone	46.03	11.08	0.71	0.00	36
SE-Nor	Norua	60.08	17.47	−0.19	0.37	25
CH-Oe1	Oensingen	47.29	7.73	0.03	0.89	30
UA-Pet	Petrodolinskoye	46.50	30.30	0.35	0.05	30
PL-wet	Polwet	52.76	16.31	−0.21	0.28	28
FR-Pue	Puechabon	43.74	3.60	0.09	0.63	35
IT-Ren	Renon	46.59	11.43	−0.05	0.79	33
DK-Lva	Rimi	55.70	12.12	0.54	0.11	10
DK-Ris	Risbyholm	55.53	12.10	0.54	0.27	6
IT-Ro2	Roccarespampani	42.39	11.92	0.06	0.72	33
IT-SRo	San Rossore	43.73	10.28	0.03	0.85	32
SE-Sk2	Skyttorp	60.13	17.84	−0.40	0.25	10
FI-Sod	Sodankylä	67.36	26.64	−0.41	0.07	20
DK-Sor	Soroe	55.49	11.65	−0.05	0.82	24
NL-Spe	Speulderbos	52.25	5.69	0.10	0.57	33
DE-Tha	Tharat	50.96	13.57	0.44	0.02	30
ES-VDA	Vall d'Alinyà	42.15	1.45	0.58	0.00	35
BE-Vie	Vielsalm	50.31	6.00	0.11	0.65	21
DE-Wet	Wetzstein	50.45	11.46	0.47	0.01	28

Table A2. Statistical analysis of the NNDMN data set and monthly IASI satellite surface concentrations comparison for each stations during 2009, 2010, 2011, 2012 and 2013. Each site is characterized by its name and coordinates, its Pearson's correlation coefficient (r) and the associated p value as well as its number of points (n). Only monthly values with a relative IASI retrieval errors below 100 % have been taken into account.

Site	Long (° E)	Lat (° N)	r	p value	n
CAU (China Agricultural University)	116.28	40.02	0.51	0.00	45
BNU (Beijing Normal University)	116.37	39.96	0.64	0.17	6
DBW (Dongbeiwang)	116.28	40.05	–	–	0
SZ (Shangzhuang)	116.18	40.14	0.72	0.00	45
BD (Baoding)	115.48	38.85	0.27	0.39	12
QZ (Quzhou)	115.02	36.87	0.32	0.03	44
YQ (Yangqu)	112.67	38.06	0.39	0.01	45
LSD (Lingshan Dao)	120.17	35.78	0.55	0.00	32
CD (Changdao)	120.74	37.91	0.58	0.00	37
YC (Yucheng)	116.63	36.92	0.42	0.12	15
ZMD (ZMD)	114.02	33.01	−0.16	0.30	45
ZZ (Zhengzhou)	113.63	34.75	0.38	0.01	43
DL (Dalian)	121.61	38.91	0.43	0.01	40
GZL (Gongzhuling)	124.82	43.50	0.52	0.00	38
LS (Lishu)	124.34	43.31	0.34	0.03	40
WY (Wuyin)	129.25	48.11	0.24	0.54	9
GH (Genhe)	121.52	50.78	−0.36	0.34	9
TFS (Tufeisuo)	87.28	43.56	0.23	0.50	11
SDS (Shengdisuo)	87.34	43.51	0.21	0.53	11
DL (Duolun)	116.49	42.20	0.52	0.29	6
BYBLK (Bayinbuluke)	84.15	43.03	0.59	0.03	14
WW (Wuwei)	102.61	37.96	−0.19	0.25	39
YL (Yangling)	108.08	34.27	0.02	0.89	45
FH (Fenghua)	121.53	29.61	0.30	0.06	38
FZ (Fuzhou)	119.57	26.06	0.02	0.92	38
WX (Wuxue)	115.94	30.07	0.47	0.01	28
BY (Baiyun)	113.27	23.16	−0.23	0.16	41
ZZ (Zhanjiang)	110.33	21.26	0.05	0.74	39
TJ (Taojiang)	112.16	28.52	0.35	0.05	33
FY (Feiyue)	113.20	28.33	0.16	0.36	35
HN (Huinong)	113.24	28.31	0.34	0.05	35
XS (Xishan)	113.18	28.36	0.47	0.00	36
NJ (Nanjing)	118.50	31.52	0.35	0.16	18
FY (Fengyang)	117.53	32.87	0.64	0.03	11
WJ (Wenjiang)	103.86	30.68	0.02	0.92	38
ZY (Ziyang)	104.63	30.13	0.58	0.00	38
YT (Yanting)	105.46	31.27	0.70	0.00	29
JJ (Jiangjin)	106.26	29.29	0.14	0.67	12
YNAU (Yunnannongda)	102.75	25.13	0.42	0.17	12
DC (Dianchi)	102.64	25.00	0.64	0.03	12
KY (Kunyang)	102.73	25.04	0.39	0.21	12
LZ (Linzhi)	94.36	29.65	−0.75	0.00	12
XN (Xining)	101.79	36.62	1.00	1.00	1

Table A3. Statistical analysis of the IDAF data set and monthly IASI satellite surface concentrations comparison for each stations during 2008, 2009, 2010 and 2011. Each site is characterized by its name and coordinates, its Pearson's correlation coefficient (r) and the associated p value as well as its number of points (n). Only monthly values with a relative IASI retrieval errors below 100 % have been taken into account.

Site	Lat (° N)	Long (° E)	r	p value	n
Banizoumbou	13.52	2.63	−0.01	0.95	47
Katibougou	12.93	−7.53	0.01	0.95	47
Agoufou	15.33	−1.48	0.06	0.73	35
Lamto	6.22	−5.03	0.39	0.01	40
Djougou	9.65	1.73	−0.04	0.81	42
Zotélé	3.25	11.88	0.22	0.18	36
Bomassa	2.20	16.33	−0.36	0.03	38
Amersfoort	−27.07	29.87	0.04	0.84	34
Louis Trischardt	−22.99	30.02	−0.15	0.43	31
Cape point	−34.35	18.48	0.05	0.84	17

Acknowledgements. IASI has been developed and built under the responsibility of the "Centre national d'études spatiales" (CNES, France). It is flown on-board the Metop satellites as part of the EUMETSAT Polar System. The IASI L1 data are received through the EUMETCast near real-time data distribution service. The research in Belgium was funded by the F.R.S.-FNRS, the Belgian State Federal Office for Scientific, Technical and Cultural Affairs (Prodex arrangement 4000111403 IASI.FLOW). M. Van Damme is grateful to the "Fonds pour la formation à la recherche dans l'industrie et dans l'agriculture" of Belgium for a PhD grant (Boursier FRIA). L. Clarisse and P.-F. Coheur are, respectively, research associate (chercheur qualifié) and senior research associate (maître de recherches) with F.R.S.-FNRS. C. Clerbaux is grateful to CNES for scientific collaboration and financial support. We gratefully acknowledge support from the project "Effects of Climate Change on Air Pollution Impacts and Response Strategies for European Ecosystems" (ÉCLAIRE), funded under the EC 7th Framework Programme (grant agreement no. 282910). Part of this research was supported by the EC under the 7th Framework Programme, for the project "Partnership with China on Space Data (PANDA)". We also would like to thanks S. Bauduin, J. Hadji-Lazaro and J.-L. Lacour as well as R. van Oss, H. Volten and D. Swart for their helpful advice.

Edited by: M. Van Roozendael

References

Adon, M., Galy-Lacaux, C., Yoboué, V., Delon, C., Lacaux, J. P., Castera, P., Gardrat, E., Pienaar, J., Al Ourabi, H., Laouali, D., Diop, B., Sigha-Nkamdjou, L., Akpo, A., Tathy, J. P., Lavenu, F., and Mougin, E.: Long term measurements of sulfur dioxide, nitrogen dioxide, ammonia, nitric acid and ozone in Africa using passive samplers, Atmos. Chem. Phys., 10, 7467–7487, doi:10.5194/acp-10-7467-2010, 2010.

August, T., Klaes, D., Schlüssel, P., Hultberg, T., Crapeau, M., Arriaga, A., O'Carroll, A., Coppens, D., Munro, R., and Calbet, X.: IASI on Metop-A: Operational Level 2 retrievals after five years in orbit, J. Quant. Spectrosc. Ra., 113, 1340–1371, doi:10.1016/j.jqsrt.2012.02.028, 2012.

Bash, J. O., Cooter, E. J., Dennis, R. L., Walker, J. T., and Pleim, J. E.: Evaluation of a regional air-quality model with bidirectional NH_3 exchange coupled to an agroecosystem model, Biogeosciences, 10, 1635–1645, doi:10.5194/bg-10-1635-2013, 2013.

Behera, S., Sharma, M., Aneja, V., and R., B.: Ammonia in the atmosphere: a review on emission sources, atmospheric chemistry and deposition on terrestrial bodies., Environ. Sci. Pollut. Res. Int., 20, 8092–131, doi:10.1007/s11356-013-2051-9, 2013.

Boersma, K. F., Jacob, D. J., Trainic, M., Rudich, Y., DeSmedt, I., Dirksen, R., and Eskes, H. J.: Validation of urban NO_2 concentrations and their diurnal and seasonal variations observed from the SCIAMACHY and OMI sensors using in situ surface measurements in Israeli cities, Atmos. Chem. Phys., 9, 3867–3879, doi:10.5194/acp-9-3867-2009, 2009.

Bouwman, A. F., Boumans, L. J. M., and Batjes, N. H.: Estimation of global NH_3 volatilization loss from synthetic fertilizers and animal manure applied to arable lands and grasslands, Global Biogeochem. Cy., 16, 1024, doi:10.1029/2000GB001389, 2002.

Boynard, A., Clerbaux, C., Clarisse, L., Safieddine, S., Pommier, M., Van Damme, M., Bauduin, S., Oudot, C., Hadji-Lazaro, J., Hurtmans, D., and Coheur, P.-F.: First simultaneous space measurements of atmospheric pollutants in the boundary layer from IASI: A case study in the North China Plain, Geophys. Res. Lett., 41, 645–651, doi:10.1002/2013GL058333, 2014.

Clarisse, L., Clerbaux, C., Dentener, F., Hurtmans, D., and Coheur, P.-F.: Global ammonia distribution derived from infrared satellite observations, Nat. Geosci., 2, 479–483, doi:10.1038/ngeo551, 2009.

Clarisse, L., Shephard, M., Dentener, F., Hurtmans, D., Cady-Pereira, K., Karagulian, F., Van Damme, M., Clerbaux, C., and Coheur, P.-F.: Satellite monitoring of ammonia: A case study of the San Joaquin Valley, J. Geophys. Res., 115, D13302, doi:10.1029/2009JD013291, 2010.

Clerbaux, C., Boynard, A., Clarisse, L., George, M., Hadji-Lazaro, J., Herbin, H., Hurtmans, D., Pommier, M., Razavi, A., Turquety, S., Wespes, C., and Coheur, P.-F.: Monitoring of atmospheric composition using the thermal infrared IASI/MetOp sounder, Atmos. Chem. Phys., 9, 6041–6054, doi:10.5194/acp-9-6041-2009, 2009.

Coheur, P.-F., Clarisse, L., Turquety, S., Hurtmans, D., and Clerbaux, C.: IASI measurements of reactive trace species in biomass burning plumes, Atmos. Chem. Phys., 9, 5655–5667, doi:10.5194/acp-9-5655-2009, 2009.

Dentener, F., Drevet, J., Lamarque, J. F., Bey, I., Eickhout, B., Fiore, A. M., Hauglustaine, D., Horowitz, L. W., Krol, M., Kulshrestha, U. C., Lawrence, M., Galy-Lacaux, C., Rast, S., Shindell, D., Stevenson, D., Van Noije, T., Atherton, C., Bell, N., Bergman, D., Butler, T., Cofala, J., Collins, B., Doherty, R., Ellingsen, K., Galloway, J., Gauss, M., Montanaro, V., Müller, J. F., Pitari, G., Rodriguez, J., Sanderson, M., Solmon, F., Strahan, S., Schultz, M., Sudo, K., Szopa, S., and Wild, O.: Nitrogen and sulfur deposition on regional and global scales: A multimodel evaluation, Global Biogeochem. Cy., 20, GB4003, doi:10.1029/2005GB002672, 2006.

EBAS: available at: ebas.nilu.no, lat access: 19 June 2014.

EDGAR-Emission Database for Global Atmospheric Research: Source: EC-JRC/PBL, EDGAR version 4.2., available at: http://edgar.jrc.ec.europa.eu (last access: 15th October 2012), 2011.

EEA-European Environment Agency: Effects of air pollution on European ecosystems: Past and future exposure of European freshwater and terrestrial habitats to acidifying and eutrophying air pollutants, available at: http://www.eea.europa.eu/data-and-maps/indicators/eea-32-ammonia-nh3-emissions-1/assessment-2 (last access: 20 August 2013), 2014.

EMEP: available at: http://www.nilu.no/projects/ccc/onlinedata/intro.html, last access: 19 June 2014.

Erisman, J. W., Bleeker, A., Galloway, J., and Sutton, M.: Reduced nitrogen in ecology and the environment, Environ. Pollut., 150, 140–149, doi:10.1016/j.envpol.2007.06.033, 2007.

Erisman, J. W., Sutton, M. A., Galloway, J., Klimont, Z., and Winiwarter, W.: How a century of ammonia synthesis changed the world, Nat. Geosci., 1, 636–639, doi:10.1038/ngeo325, 2008.

Erisman, J. W., Galloway, J., Seitzinger, S., Bleeker, A., and Butterbach-Bahl, K.: Reactive nitrogen in the environment and

its effect on climate change, Curr. Opin. Environ. Sustain., 3, 281–290, doi:10.1016/j.cosust.2011.08.012, 2011.

Erisman, J. W., Galloway, J. N., Seitzinger, S., Bleeker, A., Dise, N. B., Petrescu, A. M. R., Leach, A. M., and de Vries, W.: Consequences of human modification of the global nitrogen cycle, Philos. Trans. R. Soc. London, Ser. B, 368, 1621, doi:10.1098/rstb.2013.0116, 2013.

Ferm, M.: A Sensitive Diffusional Sampler, IVL rapport, Swedish Environmental Research Institute, 1991.

Fiore, A. M., Naik, V., Spracklen, D. V., Steiner, A., Unger, N., Prather, M., Bergmann, D., Cameron-Smith, P. J., Cionni, I., Collins, W. J., Dalsoren, S., Eyring, V., Folberth, G. A., Ginoux, P., Horowitz, L. W., Josse, B., Lamarque, J.-F., MacKenzie, I. A., Nagashima, T., O'Connor, F. M., Righi, M., Rumbold, S. T., Shindell, D. T., Skeie, R. B., Sudo, K., Szopa, S., Takemura, T., and Zeng, G.: Global air quality and climate, Chem. Soc. Rev., 41, 6663–6683, doi:10.1039/C2CS35095E, 2012.

Flechard, C. R., Nemitz, E., Smith, R. I., Fowler, D., Vermeulen, A. T., Bleeker, A., Erisman, J. W., Simpson, D., Zhang, L., Tang, Y. S., and Sutton, M. A.: Dry deposition of reactive nitrogen to European ecosystems: a comparison of inferential models across the NitroEurope network, Atmos. Chem. Phys., 11, 2703–2728, doi:10.5194/acp-11-2703-2011, 2011.

Flechard, C. R., Massad, R.-S., Loubet, B., Personne, E., Simpson, D., Bash, J. O., Cooter, E. J., Nemitz, E., and Sutton, M. A.: Advances in understanding, models and parameterizations of biosphere-atmosphere ammonia exchange, Biogeosciences, 10, 5183–5225, doi:10.5194/bg-10-5183-2013, 2013.

Fowler, D., Pitcairn, C., Sutton, M., Flechard, C., Loubet, B., Coyle, M., and Munro, R.: The mass budget of atmospheric ammonia in woodland within 1 km of livestock buildings, Environ. Pollut., 102, 343–348, doi:10.1016/S0269-7491(98)80053-5, 1998.

Fowler, D., Coyle, M., Skiba, U., Sutton, M. A., Cape, J. N., Reis, S., Sheppard, L. J., Jenkins, A., Grizzetti, B., Galloway, J. N., Vitousek, P., Leach, A., Bouwman, A. F., Butterbach-Bahl, K., Dentener, F., Stevenson, D., Amann, M., and Voss, M.: The global nitrogen cycle in the twenty-first century, Philos. Trans. R. Soc. London, Ser. B, 368, 1621, doi:10.1098/rstb.2013.0164, 2013.

Galloway, J.: The Global Nitrogen Cycle, in: Treatise on Geochemistry, edited by: Holland, H. D. and Turekian, K. K., 557–583, Pergamon, Oxford, doi:10.1016/B0-08-043751-6/08160-3, 2003a.

Galloway, J., Aber, J., Erisman, J., Seitzinger, S., Howarth, R., Cowling, E., and Cosby, B.: The Nitrogen Cascade, BioScience, 53, 341–356, 2003b.

Galloway, J. N., Townsend, A. R., Erisman, J. W., Bekunda, M., Cai, Z., Freney, J. R., Martinelli, L. A., Seitzinger, S. P., and Sutton, M. A.: Transformation of the Nitrogen Cycle: Recent Trends, Questions, and Potential Solutions, Science, 320, 889–892, doi:10.1126/science.1136674, 2008.

Gong, L., Lewicki, R., Griffin, R. J., Flynn, J. H., Lefer, B. L., and Tittel, F. K.: Atmospheric ammonia measurements in Houston, TX using an external-cavity quantum cascade laser-based sensor, Atmos. Chem. Phys., 11, 9721–9733, doi:10.5194/acp-11-9721-2011, 2011.

Hauglustaine, D. A., Balkanski, Y., and Schulz, M.: A global model simulation of present and future nitrate aerosols and their direct radiative forcing of climate, Atmos. Chem. Phys. Discuss., 14, 6863–6949, doi:10.5194/acpd-14-6863-2014, 2014.

Heald, C. L., Collett Jr., J. L., Lee, T., Benedict, K. B., Schwandner, F. M., Li, Y., Clarisse, L., Hurtmans, D. R., Van Damme, M., Clerbaux, C., Coheur, P.-F., Philip, S., Martin, R. V., and Pye, H. O. T.: Atmospheric ammonia and particulate inorganic nitrogen over the United States, Atmos. Chem. Phys., 12, 10295–10312, doi:10.5194/acp-12-10295-2012, 2012.

Hertel, O., Skjøth, C. A., Reis, S., Bleeker, A., Harrison, R. M., Cape, J. N., Fowler, D., Skiba, U., Simpson, D., Jickells, T., Kulmala, M., Gyldenkærne, S., Sørensen, L. L., Erisman, J. W., and Sutton, M. A.: Governing processes for reactive nitrogen compounds in the European atmosphere, Biogeosciences, 9, 4921–4954, doi:10.5194/bg-9-4921-2012, 2012.

Huang, X., Song, Y., Li, M., Li, J., Huo, Q., Cai, X., Zhu, T., Hu, M., and Zhang, H.: A high-resolution ammonia emission inventory in China, Global Biogeochem. Cy., 26, GB1030, doi:10.1029/2011GB004161, 2012.

IDAF: IGAC/DEBITS/AFRICA, available at: http://idaf.sedoo.fr/spip.php?rubrique38, last access: 19 June 2014.

IFFN-GFMC-16: Global Fire Monitoring Center, Global Wildland Fire Network Bulletin No. 16, available at: http://www.fire.uni-freiburg.de/GFMCnew/2011/GFMC-Bulletin-02-2011.pdf (last access: 11 April 2014), 2011.

Krupa, S.: Effects of atmospheric ammonia (NH_3) on terrestrial vegetation: a review, Environ. Pollut., 124, 179–221, doi:10.1016/S0269-7491(02)00434-7, 2003.

Leen, J. B., Yu, X.-Y., Gupta, M., Baer, D. S., Hubbe, J. M., Kluzek, C. D., Tomlinson, J. M., and Hubbell, M. R.: Fast In Situ Airborne Measurement of Ammonia Using a Mid-Infrared Off-Axis ICOS Spectrometer, Environ. Sci. Technol., 47, 10446–10453, doi:10.1021/es401134u, 2013.

Liu, X., Duan, L., Mo, J., Du, E., Shen, J., Lu, X., Zhang, Y., Zhou, X., He, C., and Zhang, F.: Nitrogen deposition and its ecological impact in China: An overview, Environ. Pollut., 159, 2251–2264, doi:10.1016/j.envpol.2010.08.002, 2011.

NADP-National Atmospheric Deposition Program: National Atmospheric Deposition Program 2011 Annual Summary, NADP Data Report 2012-01, 2012.

NASA: Fires in Eastern Russia, available at: http://earthobservatory.nasa.gov/NaturalHazards/view.php?id=51539 (last access: 1 December 2014), 2011.

Nguyen, P. and R. Hoogerbrugge, F. v. A.: Evaluation of the representativeness of the Dutch national Air Quality Network, Tech. Rep. Report 680704010/2009, RIVM, 2009.

Norman, M. and Leck, C.: Distribution of marine boundary layer ammonia over the Atlantic and Indian Oceans during the Aerosols99 cruise, J. Geophys. Res.-Atmos., 110, D16302, doi:10.1029/2005JD005866, 2005.

Nowak, J. B., Neuman, J. A., Kozai, K., Huey, L. G., Tanner, D. J., Holloway, J. S., Ryerson, T. B., Frost, G. J., McKeen, S. A., and Fehsenfeld, F. C.: A chemical ionization mass spectrometry technique for airborne measurements of ammonia, J. Geophys. Res.-Atmos., 112, D10S02, doi:10.1029/2006JD007589, 2007.

Nowak, J. B., Neuman, J. A., Bahreini, R., Brock, C. A., Middlebrook, A. M., Wollny, A. G., Holloway, J. S., Peischl, J., Ryerson, T. B., and Fehsenfeld, F. C.: Airborne observations of ammonia and ammonium nitrate formation over Houston, Texas, J. Geo-

phys. Res.-Atmos., 115, D22304, doi:10.1029/2010JD014195, 2010.

Nowak, J. B., Neuman, J. A., Bahreini, R., Middlebrook, A. M., Holloway, J. S., McKeen, S. A., Parrish, D. D., Ryerson, T. B., and Trainer, M.: Ammonia sources in the California South Coast Air Basin and their impact on ammonium nitrate formation, Geophys. Res. Lett., 39, L07804, doi:10.1029/2012GL051197, 2012.

Parrish, D. D.: Synthesis of Policy Relevant Findings from the CalNex 2010 Field Study, topospheric Chemistry Group, NOAA, available at: www.esrl.noaa.gov/csd/projects/calnex/synthesisreport.pdf, last access: 1 December 2014.

Pinder, R. W., Walker, J. T., Bash, J. O., Cady-Pereira, K. E., Henze, D. K., Luo, M., Osterman, G. B., and Shephard, M. W.: Quantifying spatial and seasonal variability in atmospheric ammonia with in situ and space-based observations, Geophys. Res. Lett., 38, L04802, doi:10.1029/2010GL046146, 2011.

Pope, III, C. A., Ezzati, M., and Dockery, D. W.: Fine-Particulate Air Pollution and Life Expectancy in the United States, N. Engl. J. Med., 360, 376–386, doi:10.1056/NEJMsa0805646, 2009.

Reis, S., Pinder, R. W., Zhang, M., Lijie, G., and Sutton, M. A.: Reactive nitrogen in atmospheric emission inventories, Atmos. Chem. Phys., 9, 7657–7677, doi:10.5194/acp-9-7657-2009, 2009.

R'Honi, Y., Clarisse, L., Clerbaux, C., Hurtmans, D., Duflot, V., Turquety, S., Ngadi, Y., and Coheur, P.-F.: Exceptional emissions of NH_3 and HCOOH in the 2010 Russian wildfires, Atmos. Chem. Phys., 13, 4171–4181, doi:10.5194/acp-13-4171-2013, 2013.

Ryerson, T. B., Andrews, A. E., Angevine, W. M., Bates, T. S., Brock, C. A., Cairns, B., Cohen, R. C., Cooper, O. R., de Gouw, J. A., Fehsenfeld, F. C., Ferrare, R. A., Fischer, M. L., Flagan, R. C., Goldstein, A. H., Hair, J. W., Hardesty, R. M., Hostetler, C. A., Jimenez, J. L., Langford, A. O., McCauley, E., McKeen, S. A., Molina, L. T., Nenes, A., Oltmans, S. J., Parrish, D. D., Pederson, J. R., Pierce, R. B., Prather, K., Quinn, P. K., Seinfeld, J. H., Senff, C. J., Sorooshian, A., Stutz, J., Surratt, J. D., Trainer, M., Volkamer, R., Williams, E. J., and Wofsy, S. C.: The 2010 California Research at the Nexus of Air Quality and Climate Change (CalNex) field study, J. Geophys. Res.-Atmos., 118, 5830–5866, doi:10.1002/jgrd.50331, 2013.

Schiferl, L. D., Heald, C. L., Nowak, J. B., Holloway, J. S., Neuman, J. A., Bahreini, R., Pollack, I. B., Ryerson, T. B., Wiedinmyer, C., and Murphy, J. G.: An investigation of ammonia and inorganic particulate matter in California during the CalNex campaign, J. Geophys. Res.-Atmos., 119, 1883–1902, doi:10.1002/2013JD020765, 2014.

Sharma, S. K., Singh, A. K., Saud, T., Mandal, T. K., Saxena, M., Singh, S., Ghosh, S. K., and Raha, S.: Measurement of ambient NH_3 over Bay of Bengal during W_ICARB Campaign, Ann. Geophys., 30, 371–377, doi:10.5194/angeo-30-371-2012, 2012.

Shen, J., Liu, X., Zhang, Y., Fangmeier, A., Goulding, K., and Zhang, F.: Atmospheric ammonia and particulate ammonium from agricultural sources in the North China Plain, Atmos. Environ., 45, 5033–5041, doi:10.1016/j.atmosenv.2011.02.031, 2011.

Shephard, M. W. and Cady-Pereira, K. E.: Cross-track Infrared Sounder (CrIS) satellite observations of tropospheric ammonia, Atmos. Meas. Tech. Discuss., 7, 11379–11413, doi:10.5194/amtd-7-11379-2014, 2014.

Shephard, M. W., Cady-Pereira, K. E., Luo, M., Henze, D. K., Pinder, R. W., Walker, J. T., Rinsland, C. P., Bash, J. O., Zhu, L., Payne, V. H., and Clarisse, L.: TES ammonia retrieval strategy and global observations of the spatial and seasonal variability of ammonia, Atmos. Chem. Phys., 11, 10743–10763, doi:10.5194/acp-11-10743-2011, 2011.

Streets, D. G., Canty, T., Carmichael, G. R., de Foy, B., Dickerson, R. R., Duncan, B. N., Edwards, D. P., Haynes, J. A., Henze, D. K., Houyoux, M. R., Jacob, D. J., Krotkov, N. A., Lamsal, L. N., Liu, Y., Lu, Z., Martin, R. V., Pfister, G. G., Pinder, R. W., Salawitch, R. J., and Wecht, K. J.: Emissions estimation from satellite retrievals: A review of current capability, Atmos. Environ., 77, 1011–1042, doi:10.1016/j.atmosenv.2013.05.051, 2013.

Sun, K., Tao, L., Miller, D. J., Khan, M. A., and Zondlo, M. A.: On-Road Ammonia Emissions Characterized by Mobile, Open-Path Measurements, Environ. Sci. Technol., 48, 3943–3950, doi:10.1021/es4047704, 2014.

Sutton, M. A., Milford, C., Dragosits, U., Place, C., Singles, R., Smith, R., Pitcairn, C., Fowler, D., Hill, J., ApSimon, H., Ross, C., Hill, R., Jarvis, S., Pain, B., Phillips, V., Harrison, R., Moss, D., Webb, J., Espenhahn, S., Lee, D., Hornung, M., Ullyett, J., Bull, K., Emmett, B., Lowe, J., and Wyers, G.: Dispersion, deposition and impacts of atmospheric ammonia: quantifying local budgets and spatial variability, Environ. Pollut., 102, 349–361, doi:http://dx.doi.org/10.1016/S0269-7491(98)80054-7, 1998.

Sutton, M. A., Tang, Y., Miners, B., and Fowler, D.: A New Diffusion Denuder System for Long-Term, Regional Monitoring of Atmospheric Ammonia and Ammonium, Water, Air Soil Pollut.: Focus, 1, 145–156, doi:10.1023/A:1013138601753, 2001.

Sutton, M. A., Nemitz, E., Erisman, J., Beier, C., Bahl, K. B., Cellier, P., de Vries, W., Cotrufo, F., Skiba, U., Marco, C. D., Jones, S., Laville, P., Soussana, J., Loubet, B., Twigg, M., Famulari, D., Whitehead, J., Gallagher, M., Neftel, A., Flechard, C., Herrmann, B., Calanca, P., Schjoerring, J., Daemmgen, U., Horvath, L., Tang, Y., Emmett, B., Tietema, A., Peuelas, J., Kesik, M., Brueggemann, N., Pilegaard, K., Vesala, T., Campbell, C., Olesen, J., Dragosits, U., Theobald, M., Levy, P., Mobbs, D., Milne, R., Viovy, N., Vuichard, N., Smith, J., Smith, P., Bergamaschi, P., Fowler, D., and Reis, S.: Challenges in quantifying biosphere-atmosphere exchange of nitrogen species, Environ. Pollut., 150, 125–139, doi:10.1016/j.envpol.2007.04.014, 2007.

Sutton, M. A., Erisman, J. W., Dentener, F., and Müller, D.: Ammonia in the environment: From ancient times to the present, Environ. Pollut., 156, 583–604, doi:10.1016/j.envpol.2008.03.013, 2008.

Sutton, M. A., Reis, S., Riddick, S. N., Dragosits, U., Nemitz, E., Theobald, M. R., Tang, Y. S., Braban, C. F., Vieno, M., Dore, A. J., Mitchell, R. F., Wanless, S., Daunt, F., Fowler, D., Blackall, T. D., Milford, C., Flechard, C. R., Loubet, B., Massad, R., Cellier, P., Personne, E., Coheur, P. F., Clarisse, L., Van Damme, M., Ngadi, Y., Clerbaux, C., Skjth, C. A., Geels, C., Hertel, O., Wichink Kruit, R. J., Pinder, R. W., Bash, J. O., Walker, J. T., Simpson, D., Horvth, L., Misselbrook, T. H., Bleeker, A., Dentener, F., and de Vries, W.: Towards a climate-dependent paradigm of ammonia emission and deposition, Philos. Trans. R. Soc. London, Ser. B, 368, 1621, doi:10.1098/rstb.2013.0166, 2013a.

Sutton, M. A., Bleeker, A., Howard, C., Bekunda, M., Grizzetti, B., de Vries, W., van Grinsven, H., Abrol, Y., Adhya, T., Billen,

G. and. Davidson, E., Datta, A., Diaz, R., Erisman, J., Liu, X., Oenema, O., Palm, C., Raghuram, N., Reis, S., Scholz, R., Sims, T., Westhoek, H., Zhang, F., with contributions from Ayyappan, S., Bouwman, A., Bustamante, M., Fowler, D., Galloway, J., Gavito, M., Garnier, J., Greenwood, S., Hellums, D., Holland, M., Hoysall, C., Jaramillo, V., Klimont, Z., Ometto, J., Pathak, H., Plocq Fichelet, V., Powlson, D., Ramakrishna, K., Roy, A., Sanders, K., Sharma, C., Singh, B., Singh, U., Yan, X., and Zhang, Y.: Our Nutrient World: The challenge to produce more food and energy with less pollution. Global Overview of Nutrient Management, Centre for Ecology & Hydrology on behalf of the Global Partnership on Nutrient Management and the International Nitrogen Initiative, 114 pp., 2013b.

Tang, Y., Cape, J., and Sutton, M.: Development and Types of Passive Samplers for Monitoring Atmospheric NO_2 and NH_3 Concentrations, The Sci. World, 1, 513–529, doi:10.1100/tsw.2001.82, 2001.

Tang, Y., Simmons, I., van Dijk, N., Marco, C. D., Nemitz, E., Dämmgen, U., Gilke, K., Djuricic, V., Vidic, S., Gliha, Z., Borovecki, D., Mitosinkova, M., Hanssen, J., Uggerud, T., Sanz, M., Sanz, P., Chorda, J., Flechard, C., Fauvel, Y., Ferm, M., Perrino, C., and Sutton, M.: European scale application of atmospheric reactive nitrogen measurements in a low-cost approach to infer dry deposition fluxes, Agr. Ecosyst. Environ., 133, 183–195, doi:10.1016/j.agee.2009.04.027, 2009.

Van Damme, M., Clarisse, L., Heald, C. L., Hurtmans, D., Ngadi, Y., Clerbaux, C., Dolman, A. J., Erisman, J. W., and Coheur, P. F.: Global distributions, time series and error characterization of atmospheric ammonia (NH_3) from IASI satellite observations, Atmos. Chem. Phys., 14, 2905–2922, doi:10.5194/acp-14-2905-2014, 2014a.

Van Damme, M., Wichink Kruit, R. J., Schaap, M., Clarisse, L., Clerbaux, C., Coheur, P.-F., Dammers, E., Dolman, A. J., and Erisman, J. W.: Evaluating four years of atmospheric ammonia (NH_3) over Europe using IASI satellite observations and LOTOS-EUROS model results, J. Geophys. Res.-Atmos., 119, JD021911, doi:10.1002/2014JD021911, 2014b.

van Pul, A., Hertel, O., Geels, C., Dore, A., Vieno, M., Jaarsveld, H., Bergström, R., Schaap, M., and Fagerli, H.: Modelling of the Atmospheric Transport and Deposition of Ammonia at a National and Regional Scale, in: Atmospheric Ammonia, edited by: Sutton, M., Reis, S., and Baker, S., 301–358, Springer Netherlands, doi:10.1007/978-1-4020-9121-6_19, 2009.

Vigouroux, C., De Mazière, M., Desmet, F., Hermans, C., Langerock., B., Scolas, F., Van Damme, M., Clarisse, L., and Coheur, P.-F.: Ground-based FTIR measurements of NH_3 total columns and comparison with IASI data, poster presented at EGU General Assembly 2013, held 7–12 April 2013 in Vienna, Austria, 2013.

Volten, H., Bergwerff, J. B., Haaima, M., Lolkema, D. E., Berkhout, A. J. C., van der Hoff, G. R., Potma, C. J. M., Wichink Kruit, R. J., van Pul, W. A. J., and Swart, D. P. J.: Two instruments based on differential optical absorption spectroscopy (DOAS) to measure accurate ammonia concentrations in the atmosphere, Atmos. Meas. Tech., 5, 413–427, doi:10.5194/amt-5-413-2012, 2012.

von Bobrutzki, K., Braban, C. F., Famulari, D., Jones, S. K., Blackall, T., Smith, T. E. L., Blom, M., Coe, H., Gallagher, M., Ghalaieny, M., McGillen, M. R., Percival, C. J., Whitehead, J. D., Ellis, R., Murphy, J., Mohacsi, A., Pogany, A., Junninen, H., Rantanen, S., Sutton, M. A., and Nemitz, E.: Field inter-comparison of eleven atmospheric ammonia measurement techniques, Atmos. Meas. Tech., 3, 91–112, doi:10.5194/amt-3-91-2010, 2010.

Wang, L. T., Wei, Z., Yang, J., Zhang, Y., Zhang, F. F., Su, J., Meng, C. C., and Zhang, Q.: The 2013 severe haze over southern Hebei, China: model evaluation, source apportionment, and policy implications, Atmos. Chem. Phys., 14, 3151–3173, doi:10.5194/acp-14-3151-2014, 2014.

Wendt, V., Wüst, S., Mlynczak, M. G., III, J. M. R., Yee, J.-H., and Bittner, M.: Impact of atmospheric variability on validation of satellite-based temperature measurements, J. Atmos. Solar-Terrest. Phys., 102, 252–260, doi:10.1016/j.jastp.2013.05.022, 2013.

Wichink Kruit, R. J., Schaap, M., Sauter, F. J., van Zanten, M. C., and van Pul, W. A. J.: Modeling the distribution of ammonia across Europe including bi-directional surface-atmosphere exchange, Biogeosciences, 9, 5261–5277, doi:10.5194/bg-9-5261-2012, 2012.

Wyers, G., Otjes, R., and Slanina, J.: A continuous-flow denuder for the measurement of ambient concentrations and surface-exchange fluxes of ammonia, Atmos. Environ. Part A. General Topics, 27, 2085–2090, doi:10.1016/0960-1686(93)90280-C, 1993.

Zhu, L., Henze, D. K., Cady-Pereira, K. E., Shephard, M. W., Luo, M., Pinder, R. W., Bash, J. O., and Jeong, G.-R.: Constraining U.S. ammonia emissions using TES remote sensing observations and the GEOS-Chem adjoint model, J. Geophys. Res.-Atmos., 118, 3355–3368, doi:10.1002/jgrd.50166, 2013.